Chapter 14

Potential Application of Photo-thermal Volumetric Ignition of Carbon Nanotubes in Internal Combustion Engines

Antonio Paolo Carlucci, Bruce Chehroudi, Antonio Ficarella, Domenico Laforgia and Luciano Strafella

Additional information is available at the end of the chapter

http://dx.doi.org/10.5772/intechopen.70887

Abstract

In internal combustion engines, an ignition source is required to initiate the combustion process. This is commonly obtained either through an electric spark generation or by physical act of compression-ignition. In order to improve performance and lower pollutants levels, researchers have proposed alternatives to conventional ignition or combustion processes, such as homogeneously-charge compression-ignition (HCCI) combustion, whose critical operational requirement is precise control of the autoignition timing within the engine operating cycle. In this work, an innovative volumetrically-distributed ignition approach is proposed to control the onset of the autoignition process, by taking advantage of the optical ignition properties of carbon nanotubes when exposed to a low-consumption light source. It is shown that this ignition method enhanced the combustion of methane, hydrogen, LPG, and gasoline (injected to chamber in liquid phase). The results for this new ignition method show that pressure gradient and combustion efficiency are increased, while combustion duration and ignition delay time are decreased. A direct observation of the combustion process indicates that these benefits are due to the spatially-distributed ignition followed by a faster initial consumption of the air/fuel mixture. The use of this ignition system is therefore proposed as a promising technology for the combustion management in internal combustion engines, specifically for the HCCI engines.

Keywords: carbon nanotubes, combustion control, internal combustion engines, metal nanoparticles, photo-thermal ignition, HCCI, autoignition, photo-ignition

1. Introduction

The system for triggering and controlling the ignition process is the heart of the robust and effective combustion process in internal combustion engines (ICEs).

The electric spark used in gasoline engines generates a relatively slow flame front, which then propagates burning the air/fuel mixture. This ignition system is, by its nature, a single point ignition system and is characterized by a relatively high energy input. The benefits of having multiple ignition nuclei and ability to vary their positions on the fuel conversion efficiency and reduction of pollutants levels have been demonstrated in the literature at different operating conditions. However, the practical applications have been limited to a few points, that is, a maximum of two spark plugs per cylinder in automotive engines.

In diesel engines, on the other hand, the ignition is achieved through the compression process, realized by the piston movement during the compression stroke. The compression ignition process, being sensitive to operating conditions such as ambient temperature and pressure, affects the following combustion development, characterized by two different burning phases. The first phase is a fast-burning combustion of the injected liquid fuel that was previously atomized, vaporized, and mixed with air during the ignition delay period, called premixed phase, which is followed by a second phase, characterized by a much slower mixture burning rate called the mixing-controlled or diffusive combustion.

In the literature, the potentials of a third combustion mode, called homogeneous-charge compression-ignition (HCCI), in simultaneously reducing fuel consumption and pollutant emissions are extensively documented. HCCI is an alternative combustion mode for ICE, in which a premixed homogeneous mixture of fuel and oxidizer (auto-)ignites, ideally all at the same time. In this manner, the combustion process instantly involves the entire mixture trapped inside the cylinder, leading to a remarkable reduction in fuel consumption [1]. The ignition (or autoignition) process in the HCCI engines exhibits multiple ignition points distributed throughout the combustion chamber. This, when combined with the combustion of a lean premixed air/fuel mixture, lowers burned-gas temperatures, which prevents the formation of nitrogen oxides (NO_x). Furthermore, combustion of premixed lean mixtures forms virtually no soot. However, the HCCI combustion mode, simple from a conceptual point of view, is hard to be implemented. In gasoline engines, waste thermal energy contained in exhaust gases and coolant, hot residuals, and internal exhaust gas recirculation (EGR) have been demonstrated to be effective ways to heat the intake air and hence initiate mixture autoignition. In this way, and under HCCI combustion mode, it is possible to achieve a reduction of the fuel consumption up to 50%, a reduction of two orders of magnitude of NO_x, comparable levels of carbon monoxide (CO), and an acceptable increase in hydrocarbons (HC)—that can be eliminated by means of an already mature technology such as the three-way catalyst—compared to conventional gasoline spark ignition engines [2].

In diesel engines, on the other hand, the critical issue is represented by the preparation of a homogeneous mixture. In this view, port injection as well as the number and timing of injections and spray and combustion chamber shape can help obtaining a more homogeneous air/fuel

mixture into the combustion chamber. The greatest benefits were reductions of NO_x and soot. However, there were little or no reductions in fuel consumption and increases in CO and HC emissions [2].

Finally, in natural gas engines, the HCCI combustion mode can be reached by increasing the intake temperature, boost pressure, and compression ratio, or varying the fuel composition (e.g., by adding n-butane).

In order to implement the above techniques, substantial modifications have been necessary on the air, exhaust, and fuel paths, as well as on the engine structure and layout. Most of all, the critical requirement for the proper operation of the HCCI engines was found to be a precise control of the autoignition process, namely, the control of the time at which autoignition of the gaseous air/fuel mixture takes place inside the combustion chamber [2, 3]. Using a variety of complex control systems, based on parameters influencing the beginning of the autoignition process, it is possible to efficiently operate a HCCI engine. However, these controlling systems are still extremely complex, expensive, and onerous [2, 4]. This stems from the fact that the onset of autoignition for premixed air/fuel mixtures is very sensitive to engine operating and design parameters. Unfortunately, the ignition processes initiated by conventional sources of external energy are sensitive to surrounding environmental conditions and generally not suitable for the HCCI engines.

Therefore, an innovative light-activated approach has been proposed by Chehroudi [3] in order to obtain a volumetrically distributed ignition. This approach, which takes advantage of the optical ignition properties of carbon nanotubes (CNTs), is based on the observation that carbon nanotubes, bounded with other nanoenergetic materials (nEMs), that is, metallic nanopowders, ignite collectively and burn when exposed to low-consumption short-duration light sources. Therefore, they could act as autoignition nuclei when mixed with a homogenous fuel/oxidizer mixture and exposed to a pulsed light source, such as an ordinary camera flash. This phenomenon is usually referred to as "photo-thermal ignition" (PTI).

A CNT is a hollow nanostructure like a hollow cage, essentially consisting of a graphitic plane rolled into a thin tube, both ends of which can be closed by a fullerene-type dome structure. The existence of CNTs was originally discovered by Iijima [5]. Since their discovery, CNTs have been a subject of intense study: this material, in fact, exhibits various interesting mechanical, thermal, optical, and electrical properties. Many of these properties have been proposed for countless applications, for example, for the hydrogen storage, as additives in structural materials and for the production of ad-hoc biosensors for the diagnosis of diseases. There are two forms of carbon nanotubes, namely single-walled carbon nanotube (SWCNT) consisting of a single layer of graphene rolled into a tube whose diameter depends on the chirality of the nanotube, and multi-walled carbon nanotube (MWCNT) that can appear in a coaxial assembly of SWCNT similar to a coaxial cable, or as a single sheet of graphite rolled into the shape of a scroll.

The mechanism by which CNTs bonded with nEMs' photo-ignite is difficult to analyze and has not been fully explained. However, there are some theories based on experimental observations. The first observation of this phenomenon was documented by Ajayan et al. [6].

They suggested that the optically black SWCNT fibers absorbed visible and infrared light and transmitted that energy as heat to Fe (iron) nanoparticle sites (leftovers from the SWCNT growth phase), which subsequently gained enough activation energy to oxidize and support a combustion reaction with the surrounding air. Tseng et al. [7] proposed that the photo-acoustic and ignition effects are attributable to rapid increase in temperature over 457°C (ignition point of Ferrocene, Fc), resulting from both absorption of the light flash by CNTs and the presence of catalyst particles in fluffy SWCNTs, generating an acoustic wave and oxidation of the CNTs. Bockrath et al. [8] showed that the phenomenon is not isolated to SWCNTs but, in fact, other carbonaceous compounds synthesized on metal catalysts can ignite upon exposure to a flash lamp. Braidy et al. [9] not only confirmed the flash ignition effect on SWCNTs but also reported the presence of iron oxide particles in the combustion by-products. In [10], the authors concluded that the metal nanoparticle impurities in the SWCNT samples are responsible for the photo-ignition phenomenon.

Despite the intensive analysis of the PTI phenomenon, few applications have been proposed so far. Among them, the idea of igniting various fuel/oxidizer mixtures through PTI has rather been investigated. For example, Berkowitz et al. [11] introduced and mixed SWCNTs (containing 70% iron by weight) in an air/ethylene mixture inside a combustion chamber and exposed them to the camera flash, triggering in this way the combustion process. Another application was proposed by Manaa et al. [12] who demonstrated that the flash ignition and initiation of explosive-nanotubes mixture—SWCNTs with at least 29% by weight of iron impurity—in solid fuels are possible. However, in order to attain SWCNTs-nEMs mixture photo-ignition in liquid fuels, the CNTs-nEMs must be separated from the liquid until the moment of ignition. Badakshan et al. [13] have encapsulated a small sample of SWCNTs and solid additives—aluminum nanoparticles and ammonium perchlorate as solid oxidizers—inside a gelatin capsule through which they have been flashed. It was observed that the photo-ignition of nanopowder speeded up the combustion process of hexane + acetone as fuels (50% each). Furthermore, the authors have also tested PTI of simulated solid rocket fuel as an alternative to classic electric ignition. These tests essentially showed a great potential for obtaining the volumetrically distributed ignition of liquid and solid fuels.

A further application was first pioneered by Chehroudi [14], who studied the PTI of liquid fuels with CNTs, was limited to atmospheric conditions. Chehroudi [15–20] believes that this phenomenon could be used to ignite multiple points in an air/fuel mixture simultaneously, for example in ICE, and hence realizing the so-called volumetrically-distributed ignition for HCCI combustion.

The use of PTI system would lead to the following advantages compared to the other ignition systems:

- the ignition could be achieved remotely and timely; and
- the volume where ignition takes place can be adjusted to achieve both localized or volumetrically distributed ignition.

A first investigation in this direction has been described in [21, 22], where the combustion process initiated by CNT and nEMs, collectively referred to as nanoignition agents (nIAs),

when exposed to a light source, was compared with the one obtained with a conventional spark plug ignition system (SI), limiting the analysis only to air/methane mixtures. For all air/fuel ratios (AFRs) tested, it was demonstrated that the combustion triggered by PTI of the MWCNTs with Fc (i.e., Ferrocene) was characterized by a higher combustion pressure gradient and a higher peak pressure than the one started by the SI. Moreover, a volumetrically distributed combustion process was observed instead of the classic flame front propagation seen in conventional gasoline engines. Therefore, in this chapter, the application of "CNT bounded with nEMs powders," collectively referred here as nanoignition agents (nIAs), for the ignition of different fuels such as methane (CH_4), liquified petroleum gas (LPG), hydrogen (H_2), and gasoline, inside a constant volume chamber is described. A constant volume chamber was used to simulate the combustion chamber of an ICE, highlighting the benefits, in terms of reduction of combustion duration and its completeness, compared with the combustion triggered by a conventional SI system.

2. Experimental setup

A system was designed and realized on purpose to demonstrate volumetric ignition of gaseous fuels (methane, hydrogen, and LPG) and gasoline through PTI of MWCNTs with 75% by weight of Fc (it was demonstrated in [23] that this composition had the lowest power density required for ignition). MWCNTs and Fc properties are reported, respectively, in **Table 1**. A schematic diagram of the complete experimental layout for both air/gaseous fuel mixtures and air/gasoline mixtures is shown in **Figure 1**.

	MWCNTs	**Fc**
Purity	≥98%	98%
Form, color	Powder, black	Powder, yellow-orange
O.D. × I.D. × L.	10 nm ± 1 nm × 4.5 nm ± 0.5 nm × 3–6 μm	–
Density	~2.1 g/mL at 25°C (lit.)	1.49 g/cm^3
Bulk density	0.068 g/cm^3	–
Surface area	280–350 m^2/g	–
Melting point	3652–3697°C (lit.)	172–175°C (lit.)
Specific heat (~300 K)	242 kJ/kg	344 kJ/kg
Autoignition point	–	>150°C
Boiling point	–	249°C (lit.)
Vapor pressure	–	0.03 mmHg (40 °C)
Absorption	–	λ_{max} = 358 nm

Table 1. Properties of MWCNTs and ferrocene.

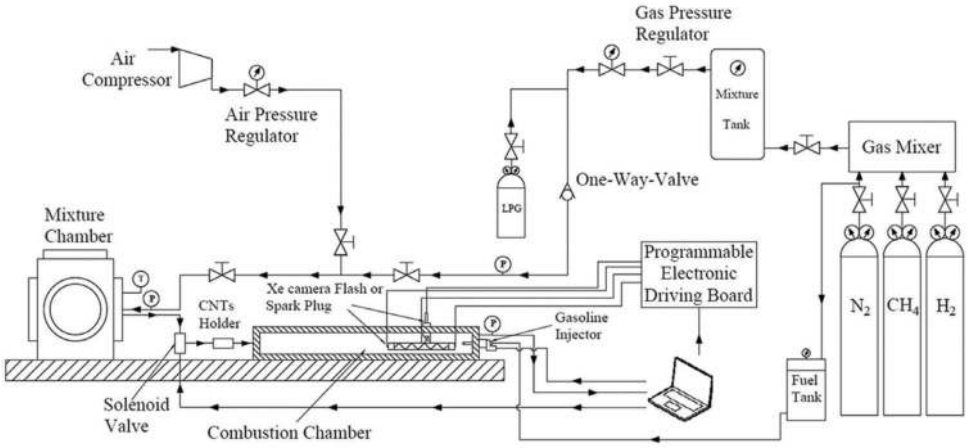

Figure 1. Schematic diagram of the experimental apparatus used during air/gaseous fuels and air/gasoline tests. Reprinted from [24], with permission from Elsevier.

The experimental setup was designed for performing a single combustion event at a time; the procedure for charging the air/fuel mixture as well as the ignition agents, therefore, must be repeated for each test, as detailed in the following. The constant volume combustion chamber is made of low-carbon steel and has a cylindrical shape with inner diameter of 53 mm and length of 270 mm. The chamber was equipped with a piezoresistive pressure sensor (KELLER type PA-21Y 0–200 bar). Pressure signal has been sampled at 2.5 kHz using a NI cDAQ 9178 acquisition board with a NI 9205 AI module. A longitudinal quartz rectangular optical window (172 mm length × 37 mm height × 20 mm thickness) was mounted along the side of the combustion chamber to allow visual access. By using a CCD Memrecam GX-1F High Speed framing camera, positioned in front of the quartz optical access, images of the ignition and burning processes have been acquired with a frame rate of 2.5 kHz.

An automotive spark plug (NGK model 4983 DCPR7E-N-10) and a Xe camera flash (Linear Xenon Flash Tubes model FT-L4040 for air/gaseous fuel tests, and a Linear Xenon Flash Tubes model FT-L6085 for air/gasoline tests) have been placed at appropriate locations inside the combustion chamber. In this manner, the combustion process via SI can be compared with that obtained through PTI of MWCNTs/nEMs mixed with air/fuel mixture. Both ignition methods have been activated by a relay, remotely controlled by means of a DIO 5 Volt TTL High Speed NI 9401 module. Once the desired pressure of 3 bar is reached in the combustion chamber, the solenoid valve automatically closes and, after a constant delay, a TTL signal is generated for activating either the camera flash or the spark plug. The maximum energy that can be released by Xe flash lamps used for photo-ignition is respectively 50 J for tests with gaseous fuels and 120 J for tests with gasoline since, supposedly, tests with gasoline would require more energy for nIAS ignition.

In order to run the experiments for air/gaseous fuel mixtures, air and gaseous fuel are separately introduced into the mixture chamber through different ducts. The amount of gaseous

fuels used in each case is determined in order to ensure a final pressure of 6 bar in the mixture chamber while at the same time achieve a desired air/gaseous-fuel mass ratio. From the mixture chamber, the air/gaseous-fuel mixture is introduced into the combustion chamber. A solenoid valve is used to determine the amount of air/gaseous fuel mixture introduced into the combustion chamber in order to reach a desired pressure of 3 bar at the onset of the experiment. Passing through the solenoid valve, the mixture flow also picks up and carries with it a desired amount of MWCNTs/nEMs (nIAs) into the combustion chamber previously introduced in the CNTs holder, see **Figure 1**.

For the experiments carried out with air and gasoline, a liquid fuel injection system composed of a fuel tank pressurized with an inert gas (nitrogen) to a value equal to 4.5 bar is used for all tests. The fuel injection system is composed of a traditional automotive gasoline injector and a module to control the injector opening. In order to run the experiments, air and gasoline are separately introduced into the combustion chamber. The amount of the gasoline introduced into the combustion chamber is determined in order to ensure a desired value of the air/gasoline mass ratio and this is realized through on the pulse width applied to the electronics associated with the injector control system. Once the gasoline is injected into the combustion chamber, the air, at a pressure of 6 bar in the mixture chamber, is introduced into the combustion chamber by means of a solenoid valve. In this case too, the amount of air introduced into the combustion chamber is controlled by the opening time of the solenoid in order to reach the desired pressure of 3 bar for each test. Tests with the gasoline fuel were conducted by varying an additional parameter, that is, the "residence time" of the liquid gasoline injected into the combustion chamber before it is mixed with the air coming from the mixture chamber carrying the nIAs. Because the photo-ignition could possibly be negatively impacted due to wetting of the nIAs by the injected liquid gasoline spray, the effects of this residence time should offer a preliminary data as to the impacts of such a wetting process. The residence time is the time between the end of liquid fuel injection and the air solenoid valve opening time. Two different residence times have been tested: 0 and 500 ms, representing the lower and upper bounds for this parameter used in this study.

For each test, as described previously, once the desired pressure (3 bar) was reached in the combustion chamber, the solenoid valve was automatically closed and, after a constant delay, a TTL signal was generated for activating either the camera flash or the spark plug. Furthermore, the energy released by the flash unit was about 5 J for air-methane fuel tests (this value was assumed to be constant and taken as a reference for all air-gaseous fuel tests), 8 J for air-gasoline tests, while the energy released by the spark plug was about 20 J for all tests.

Before each test, the combustion chamber was thoroughly purged with fresh air. In all the tests, nIAs sample, each consisting of 20 mg of MWCNTs with 75% of Fc by weight were used. The minimum amount of nanoparticles was obtained as in [22], which corresponds to a nIAs concentration of 159 ppmv in the combustion chamber. Out of 158 ppmv, 139 represented by the MWCNTs and 19 ppmv by the Fc, corresponds to an overall energy equal to 6.3 J, of which 1.1 J come from MWCNTs and 5.2 J from Fc (which collectively are less than 1% of the overall thermal energy released by the fuels).

For experiments with both ignition systems, tests were conducted by varying the relative air/fuel ratio, λ, defined as:

$$\lambda = \frac{(A/F)_{act}}{(A/F)_{st}} \tag{1}$$

where $(A/F)_{act}$ is the ratio between air (A) and fuel (F) mass actually fed into the combustion chamber, and $(A/F)_{st}$ is the stoichiometric amount of air for the type of the fuel per unit amount of fuel used. Based on this definition, $\lambda = 1$ represents an actual stoichiometric mixture, while $\lambda > 1$ indicates a mixture leaner than the stoichiometric as λ exceeds unity. In this work, $(A/F)_{st}$ for methane, hydrogen, LPG, and gasoline were assumed equal to 17.4, 34, 15.5, and 14.7, respectively. The air/fuel ratio, λ, was varied within an interval ranging from 1 to 3.5 and was estimated considering both the mixture composition in the mixture chamber and the filling process of the combustion chamber described earlier.

The ignition and combustion characteristics were analyzed through measurement of the combustion chamber pressure. In fact, for a constant volume chamber and under the hypotheses of homogeneous system and negligible wall heat transfer, the first law of thermodynamics allows the estimation of the heat release rate (*HRR*) by the fuel combustion as:

$$HRR(t) = \frac{dQ}{dt} = \frac{1}{\gamma - 1} V \frac{dp}{dt} \tag{2}$$

where Q is the heat released by the fuel during combustion (on first approximation, it is proportional to the fuel burned), γ is the mixture-specific heat ratio (assumed constant and equal to 1.38), V is the combustion chamber volume, and p is the pressure measured in the combustion chamber. Using the *HRR*, it is also possible to estimate the cumulative thermal energy released within a time interval between the start of combustion ($t_{ignition}$) and any time t later as follows:

$$cumHRR(t) = \int_{t_{ignition}}^{t} HRR\,dt \tag{3}$$

The maximum value of the *cumHRR(t)* is obtained by integrating the *HRR* between $t_{ignition}$ and the time t_{pmax}, which corresponds to the maximum pressure reached in the combustion chamber. This value is an indicator of the total heat released. Furthermore, knowing *cumHRR(t)*, it is also possible to estimate the combustion efficiency, here defined as:

$$\eta_b = \frac{\int_{t_{ignition}}^{t_{p\max}} HRR\,dt}{\left(m_{fuel}{}^{*} H_{i,fuel}\right) + \left(m_{nIAs}{}^{*} H_{i,nIAs}\right)} \tag{4}$$

in which the numerator is equal to the total heat released during combustion, while the denominator is equal to the thermal energy supplied to the system in the form of liquid or gaseous fuels. The contribution of the nanoparticles combustion energy in the denominator is equal to 6.3 J, which is less than 0.3% for each condition tested, and has been neglected.

Figure 2 shows *cumHRR* traces of the fuel burning process when initiated through the ignition of nIAs via a flash and a spark plug in an air/methane mixture at a λ value of 1.6. It is possible to see that, after the trigger signal (flash or spark activation), both curves exhibit a rising phase due to the heat released by the fuel during the combustion and reach a peak value when all the fuel is fully oxidized. Afterward, the pressure, and *cumHRR* as a consequence, slowly

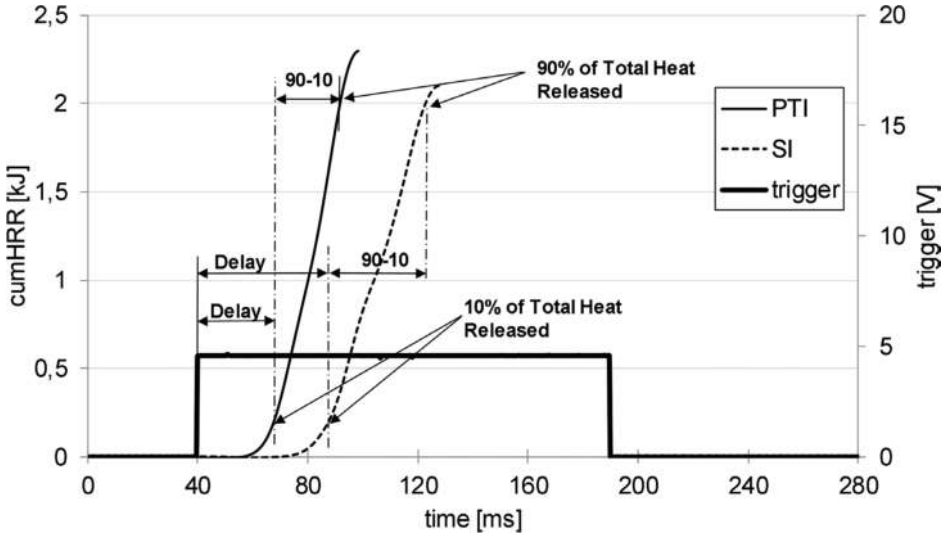

Figure 2. *cumHRR(t)* traces for PTI and SI ignition approaches using air/methane mixture at $\lambda = 1.6$. Reprinted from [24], with permission from Elsevier.

decreases (not shown in **Figure 2**) due to cooling of the exhaust gases through heat exchange with the chamber walls. Therefore, the portion of the *cumHRR(t)* curve useful for the combustion analysis is only the rising one as shown.

From the *cumHRR(t)* curve, it was possible to estimate the following parameters:

- the *ignition delay*, defined as the difference between the time when the amount of heat released had reached a value equal to 10% of total heat released and the time when the trigger has been activated;
- the *combustion duration*, defined as the difference between the time instants when the heat released had reached 90% and 10% of the total heat released. Note that the "total" combustion period is the sum of ignition delay and combustion duration.

3. Performance of PTI combustion

3.1. Air/gaseous fuel mixtures

In **Figure 3**, the *cumHRR(t)* curves related to PTI (a, a′, and a″) and SI (b, b′, and b″) combustion processes are shown. **Figure 3** also separates results for methane, LPG, and hydrogen for different values of λ. **Table 2** shows percentages of CNT and Fc for different fuels and different values of λ in the tests.

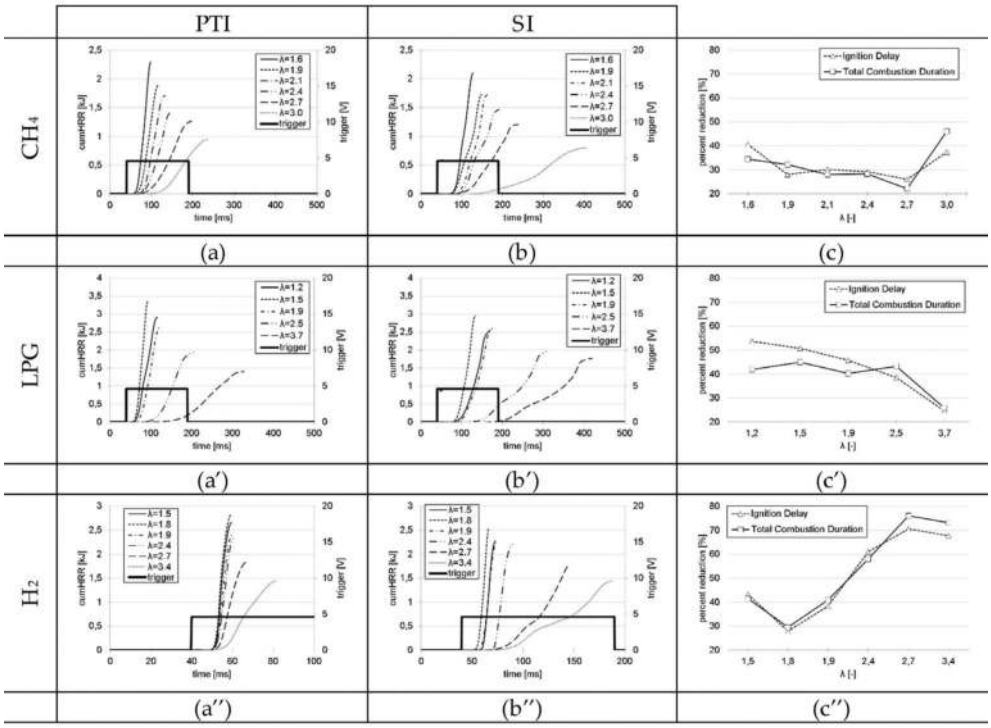

Figure 3. Plots of *cumHRR(t)* for PTI (a, a′, and a″) and SI (b, b′, and b″) ignition methods are shown. Plots in (c, c′, and c″) show percent reductions of ignition delay and total combustion duration for the PTI approach with respect (or reference) to the SI method for different values of λ. Results for methane, LPG, and hydrogen are shown. PTI and SI stand for photo-thermal ignition and spark ignition. Reprinted from [24], with permission from Elsevier.

Comparing the results for PTI column with those for SI column in **Figure 3**, it can be observed that the combustion initiated by the photo-thermal ignition of nIAs releases a total heat higher than the case in which the mixture is ignited by a spark plug. This effect is thought to be due to two reasons. On one hand, the wall heat transfer is expected to play a role in SI due to longer combustion duration. On the other hand, from the analysis of combustion process images (results are presented in the following section), the combustion triggered by the PTI involves the entire mixture in the combustion chamber when compared to the SI case. It is therefore expected that for the PTI case, the mixture at the peripheral areas of the combustion chamber (i.e., near-wall regions) is more easily reached and burned. While for the SI combustion, this would be unlikely because the propagating flame front cools as it approaches the walls of the chamber. Moreover, comparing results in PTI and SI columns in **Figure 3**, it can also be argued that, with PTI, both ignition delay and combustion duration are shortened. This conclusion is confirmed by results reported in **Figure 3(c)**, (**c**′), and (**c**″) for methane, LPG, and hydrogen, respectively, which show percent relative reductions in ignition delay and total combustion duration using PTI as compared to the SI approach. The same trend has also been reported in [11] where the authors have tested the photo-induced

	Methane						LPG					Hydrogen					
λ [−]	1.6	1.9	2.1	2.4	2.7	3.0	1.2	1.5	1.9	2.5	3.7	1.5	1.8	1.9	2.4	2.7	3.4
Air [g]	1.73	1.75	1.76	1.77	1.77	1.78	1.79	1.80	1.806	1.82	1.83	1.44	1.49	1.52	1.57	1.59	1.64
Fuel [g]	0.06	0.05	0.05	0.04	0.04	0.03	0.09	0.08	0.06	0.05	0.03	0.03	0.03	0.02	0.02	0.02	0.01
% CNT	0.28	0.28	0.28	0.28	0.28	0.28	0.27	0.27	0.27	0.27	0.27	0.34	0.33	0.32	0.31	0.31	0.30
% Fc	0.84	0.83	0.83	0.83	0.83	0.82	0.8	0.8	0.8	0.8	0.8	1.00	0.99	0.97	0.95	0.93	0.90

Table 2. Air, gaseous fuel, CNT and Fc quantities used for each test. Percentages are on mass basis.

http://dx.doi.org/10.5772/intechopen.70887

ignition of quiescent air/fuel mixtures containing suspended photo-sensitive nanomaterials. SWCNTs with 70% Fe impurity by weight were suspended in air/ethylene mixtures in a static combustion chamber and exposed to a camera flash to cause ignition of the mixture. For comparison purposes, traditional automotive spark ignition experiments were also carried out for air-ethylene mixtures.

Still referring to **Figure 3**, and for all gaseous fuel tests, increasing λ, the maximum *cumHRR(t)* decreases and is delayed. In fact, the combustion processes are limited in their heat capacity by the amount of air mixed with the gaseous fuel. Therefore, the maximum gaseous fuel amount is determined based on the maximum amount of air that the system is capable of handling. It is possible to note that the maximum *cumHRR(t)* value is higher at the near-stoichiometric ratio and decreases at higher λ values. This is because the amount of air to complete the combustion process is more than that necessary for the stoichiometric AFR (λ = 1). For all conditions tested, the combustion process with hydrogen is much faster, more intense, and shows a shorter ignition delay and combustion duration compared to other two gaseous fuels. This is mainly due to its laminar flame burning speed, being higher than that of methane and LPG (see data reported in **Table 3**), and more intense because the lower heating value (LHV) of hydrogen is higher than that of methane and LPG. Finally, the ignition delay is shorter because the minimum ignition energy required to ignite hydrogen is ≈0.02 mJ, while those for the methane and LPG are 0.3 and 0.26 mJ, respectively.

From **Figure 3(c)**, (**c**′), and (**c**′′), it can be seen that in all cases, the ignition delay period is reduced when combustion was initiated using the PTI approach. Interestingly, it can also be observed that, for the methane and LPG, the advantage (in terms of % reduction in ignition delay period and total combustion duration) of PTI declines as the mixture AFR increases toward the leanest mixture. There is an exception in the case of methane and for the leanest mixture tested where this percent reduction actually increases substantially (from λ of 2.7–3.0). One sees a completely different trend for hydrogen, where the advantage of the photo-ignition continuously increases as the mixture is leaned out. The comparison of the percent reductions in ignition delay period to those for the total combustion duration indicates that the two values are generally very close to each other. This suggests that the benefits of PTI are primarily at the ignition delay phase of the combustion. However, one can see a slightly larger difference between the two values for LPG and only for the lowest values of the λ.

	Hydrogen	**Methane**	**LPG**
LHV [mJ/kg]	119.9	50.0	46.2
Flammability limit	2.9–76%	5.3–15%	1.7–9.5%
Flash point [°C]	585	540	480
Minimum ignition energy [mJ]	0.02	0.30	0.26
Laminar flame speed [m/s]	2.7–3.3	0.3–0.4	0.3–0.4

Table 3. Physical properties of tested gaseous fuels.

http://dx.doi.org/10.5772/intechopen.70887

The combustion peak pressures reached inside the combustion chamber, using both the PTI and SI methods, are reported in **Figure 4(a)**, (**b**), and (**c**), for methane, LPG, and hydrogen, respectively. Also, the total combustion duration and ignition delay times are shown in **Figure 4(a′)**

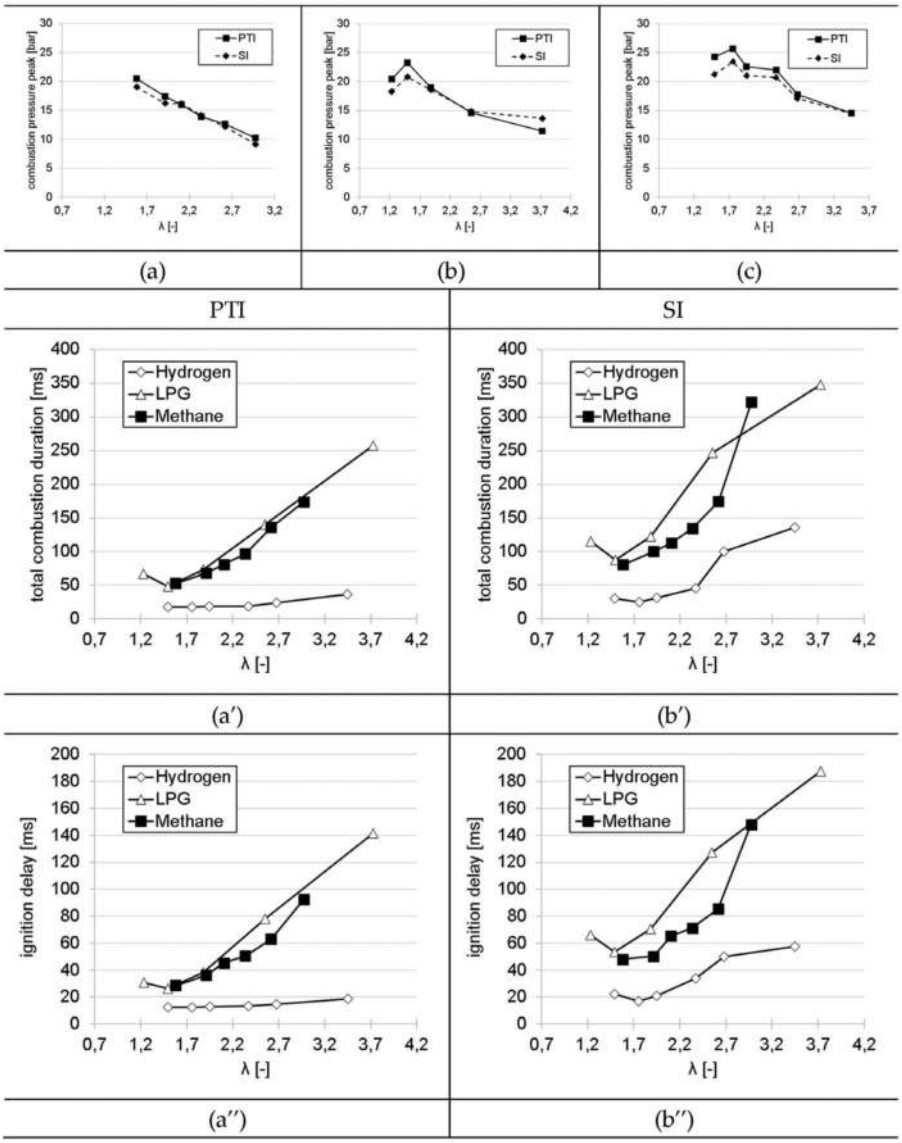

Figure 4. Comparison of the peak pressures a, b, and c for CH_4, LPG, and H_2, respectively. Total combustion duration (a′) and ignition delay (a″) with PTI and total combustion duration (b′) and ignition delay (b″) with SI for different values of λ are shown for the gaseous fuels used in this study. Reprinted from [24], with permission from Elsevier.

and (**a**″) for the PTI and **Figure 4(b′)** and (**b**″), for the SI approaches. In this way, differences between the three gaseous fuels are highlighted.

In summary, rapid rise of pressure and, therefore, a shorter pressure rise time, as well as a higher total heat released are seen in **Figure 3**. Also, mostly higher peak pressures were observed for the PTI approach as seen in **Figure 4**. This is due to the fact that the ignition of the mixture by flash exposure of the MWCNTs/nEMs leads to numerous ignition nuclei, burning "simultaneously," and hence speeding up the heat release during the combustion process. However, with the spark plug approach, as it is well known, the combustion process is triggered in only one point (i.e., within the spark plug gap) and then proceeds with the propagation of a flame front. The fuel mixture burning process is therefore too far from burning simultaneously as it is almost the case for the PTI.

This spatially-distributed ignition of the air/fuel mixture has been confirmed by observing the combustion process directly. **Figure 5** shows consecutive frames of the combustion process evolution in time. Two series of pictures related to the combustion process with PTI (left column) and spark plug (right column) are reported. Data refer to λ = 2.10 for air/methane mixture, and the time interval between two consecutive frames is equal to 5 ms. It is clearly visible that, with PTI process, the combustion is faster and the combustion chamber is entirely illuminated starting from the fifth frame indicating spatial burning. On the contrary, in the SI case, the propagation of a flame front is recognized in all the pictures. Moreover, the light radiated by the flame is weaker.

Finally, in **Figure 6**, the combustion efficiency η_b with PTI and SI is reported for different values of λ for CH_4, LPG, and H_2. It is possible to note that, for each gaseous fuel tested, the

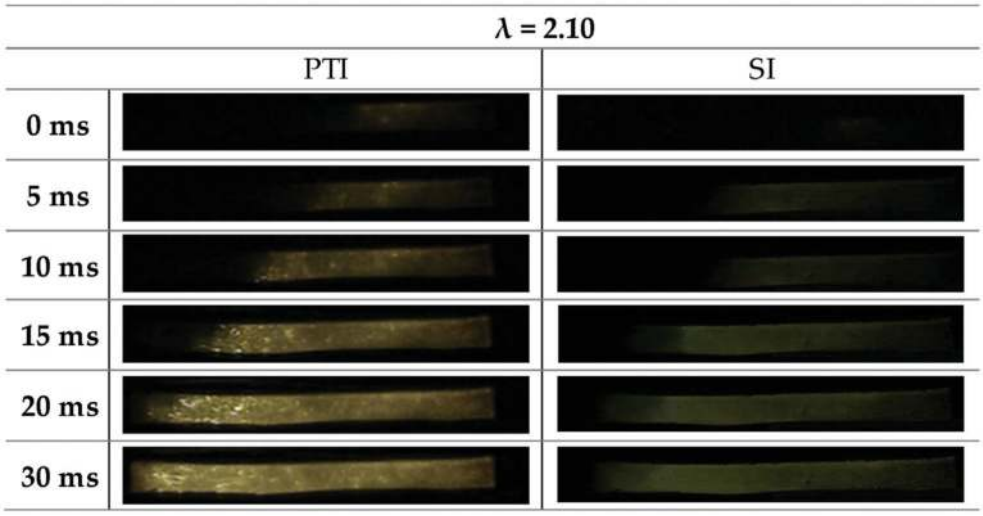

Figure 5. Pictures of the combustion process of an air/methane mixture with λ = 2.10; comparison between PTI and SI. Reprinted from [21], with permission from Elsevier.

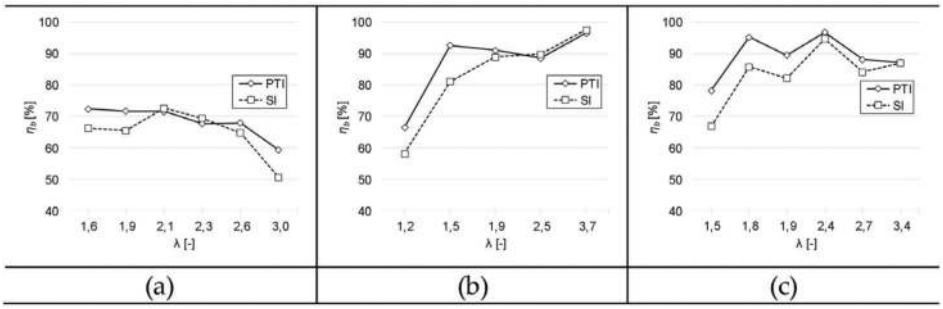

Figure 6. Comparison of combustion efficiency with PTI and SI at different values of λ and for (a) CH_4, (b) LPG, and (c) H_2.

combustion efficiency obtained with the combustion process triggered by the PTI process is slightly higher or comparable to that observed using the spark plug.

3.2. Air/gasoline mixtures

For the first time, the feasibility of igniting air/gasoline mixtures by means of PTI has been demonstrated in a constant volume combustion chamber. The combustion process has been compared with the one obtained by a traditional SI system. For these tests too, the amounts of air and gasoline as well as the CNT and Fc as percentages of the fuel mass in the mixture have been calculated, and are reported in **Table 4**.

Figure 7(a) and (**b**) show *cumHRR(t)* traces for tests with liquid gasoline fuel injection by using PTI and SI approaches, respectively. Results for the percent reduction of combustion duration and ignition delay time using PTI as compared to SI approach are also shown in **Figure 7(c)** and (**c**′). Data shown in **Figure 7(a)**, (**b**) and (**c**) are related to tests when the residence time of gasoline fuel inside the combustion chamber (before mixing with the incoming air through the solenoid valve) was equal to 0 ms. On the other hand, results reported in **Figure 7(a′)**, (**b**′) and (**c**′) refer to tests with the residence time 500 ms. In the first set of tests, the liquid fuel, after injection into the combustion chamber, was immediately mixed

λ [–]	Air [g]	Gasoline [g]	% CNT	% Fc
0.4	1.97	0.34	0.22	0.65
0.5	1.97	0.26	0.22	0.67
0.8	1.97	0.16	0.23	0.70
1.2	1.97	0.11	0.24	0.72
2.2	1.97	0.06	0.25	0.74
2.7	1.97	0.05	0.25	0.74

Table 4. Air, gasoline, CNT and Fc quantities used of each test. Percentages are on mass basis.

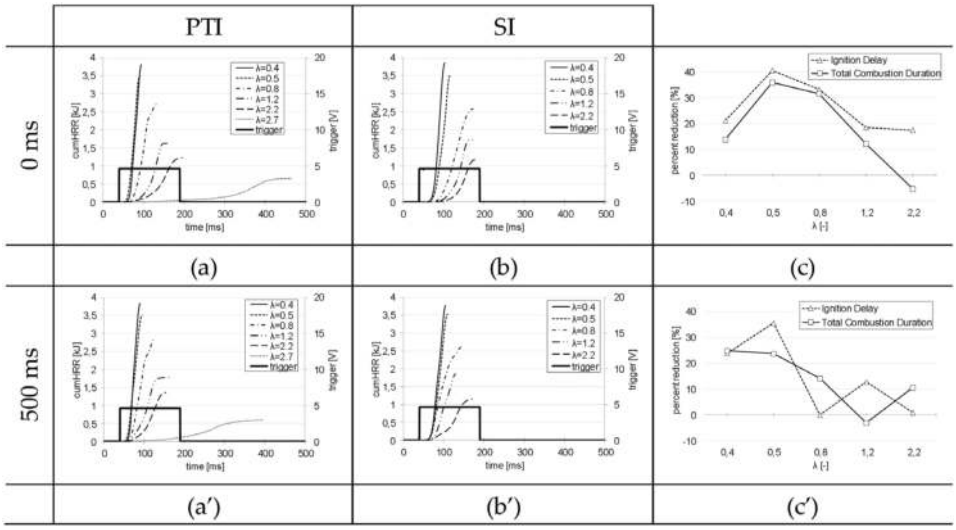

Figure 7. *cumHRR(t)* for combustion of liquid gasoline injection into the chamber initiated with PTI (a, a′) and SI (b, b′) for different values of λ and at two residence times of 0 and 500 ms. Percent reduction of the ignition delay and total combustion duration (c, c′) with PTI as compared to the SI approach for different values of λ and at two residence times of 0 ms and 500 ms are shown. Reprinted from [24], with permission from Elsevier.

with the air coming from the mixture chamber. In the second set of tests, the mixing process inside the combustion chamber took place after a fuel residence time equal to 500 ms before the air from the mixture chamber is brought into the combustion chamber. Note that because the gasoline is injected into the combustion chamber in liquid phase, the case with zero residence time implies ignition in the presence of fuel which is predominantly in liquid phase. The case with 500 ms attempts to allow time for more vaporization/mixing to approach a more homogenous mixture. However, the degree of mixing and homogeneity cannot be fully verified at this time.

Also in tests with the liquid fuel, it was observed that the combustion process triggered by the photo-thermal ignition system exhibited the same trend seen when gaseous fuels were used. That is, the combustion process triggered by the PTI generated higher or comparable *cumHRR* to that observed with the spark plug ignition system. Increasing λ, i.e., burning leaner mixtures, the peak *cumHRR* decreases and is delayed. Furthermore, it is seen in **Figure 7(c)** and (**c**′) that with PTI, both ignition delay and total combustion duration are shorter than those calculated when SI is used.

From **Figure 7**, it can also be noted that the combustion process for a very lean condition, that is, a λ value equal to 2.7, has occurred only for the photo-thermal ignition process, while a misfire took place when combustion was initiated by the spark plug system. This misfire could be either due to an excess of air in the air/fuel mixture or the nature of the SI process. Because the spark plug can only provide ignition at a single point, it is intrinsically incapable of initiating and sustaining the flame front under such a highly lean condition.

http://dx.doi.org/10.5772/intechopen.70887

From **Figure 8**, it is possible to note that the combustion efficiency obtained with the combustion process triggered by photo-thermal ignition is slightly higher or comparable to that observed using the spark plug, for both residence times used in this study.

Figure 9 shows (a) peak pressure, (b) ignition delay, (c) combustion duration, and (d) combustion efficiency, for different values of λ and for the two residence times tested. Generally, it is seen that the combustion process generated for the longer residence time exhibits a higher peak of combustion pressure. The ignition delay for the tests with 500 ms residence time seems to be equal or less than the ones with 0 ms case. However, both ignition delay and combustion duration with 500 ms residence time are shorter compared to those at 0 ms. Furthermore, it was possible to note a slight improvement of the combustion efficiency and the total heat released (THR) for the tests carried out igniting the mixtures where the fuel has had a higher residence time before mixing with the air. This behavior could be due to more time for evaporation of the gasoline fuel droplets in the combustion chamber after liquid injection, leading to a more homogeneous and distributed air/fuel mixture inside the combustion chamber. This could facilitate the ignition process and cause a faster consumption of the air/gasoline mixture with a consequent increase of the combustion peak pressure and efficiency.

Finally, in each test with PTI, shorter pressure rise times and higher peaks of *cumHRR* and combustion pressures were observed because the ignition of the mixture was by a large number of ignition nuclei which occurred "simultaneously," thereby speeding up the combustion process. With the spark plug ignition system, combustion is initiated at single point and hence proceeds with flame propagation mechanism. The burning process is therefore far from being "simultaneous." This behavior has been confirmed by observing the combustion process through high-speed imaging. **Figure 10** shows high-speed images of a single combustion event in each case, initiated by the two ignition systems. Two series of pictures related to the combustion process with PTI (left column) and SI (right column) are reported. It is possible to note that even from the first frame an instantaneous and spatially

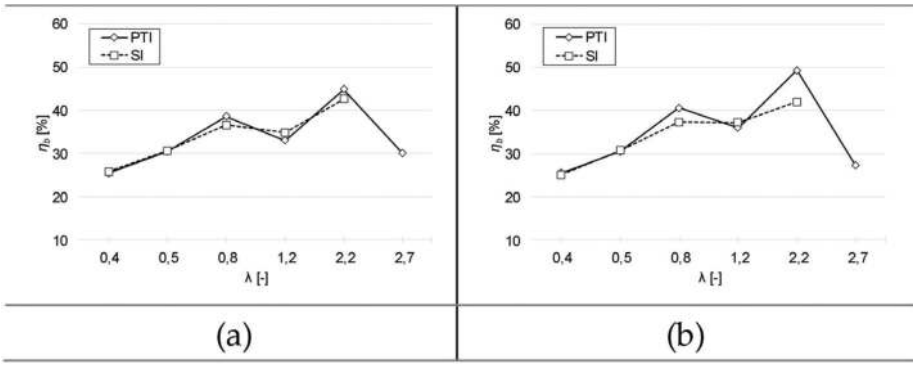

Figure 8. Combustion efficiency with PTI and SI for different values of λ and for tests carried out with a residence time equal to 0 ms (a) and 500 ms (b).

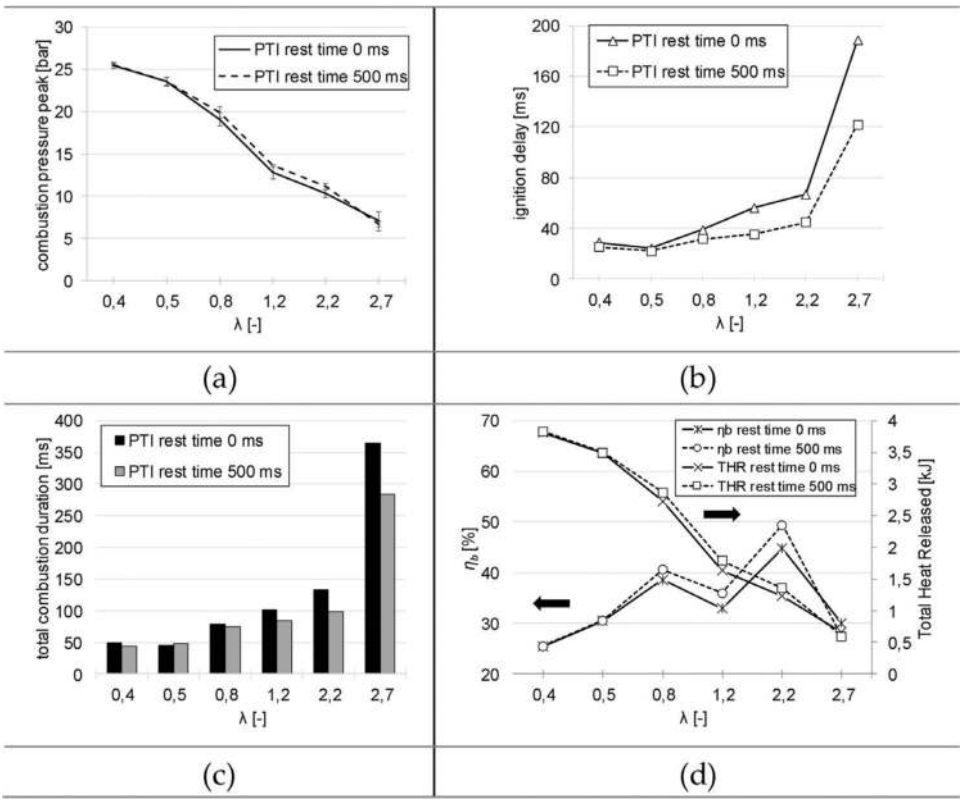

Figure 9. Comparison of (a) peak pressure, (b) ignition delay, (c) total combustion duration, (d) combustion efficiency, and total heat released with PTI for different values of λ and for tests carried out with a residence time equal to 0 and 500 ms are shown.

distributed MWCNTs/nEMs particles ignition is occurring during the flash exposure, which leads to ignition of the entire charge in the combustion chamber. Indeed, the combustion chamber is fully illuminated starting from the third frame. The light radiated by the burning process is distributed throughout the entire chamber until the combustion process is completed. This could be due to the fact that the nanoignition agents, being spatially distributed inside the chamber, are able to ignite the mixture away from the actual location of the flash lamp ignition source. On the other hand, the combustion process triggered by the spark plug exhibits an ignition phase that is longer and filled by the presence of flame starting from the 5th to 6th frame. It initially involves only a small fraction of the charge within the chamber (i.e., near the spark plug electrodes) with the high-intensity areas located close to the trigger point (i.e., spark plug). The spark ignition process forms a flame kernel which subsequently propagates and consumes the fuel at the burning speed of the flame. Note that the air/gasoline ratio for **Figure 10** is at a rich mixture condition because it generates a much better contrast. However, images under lean condition also exhibited very similar burning behavior explained here.

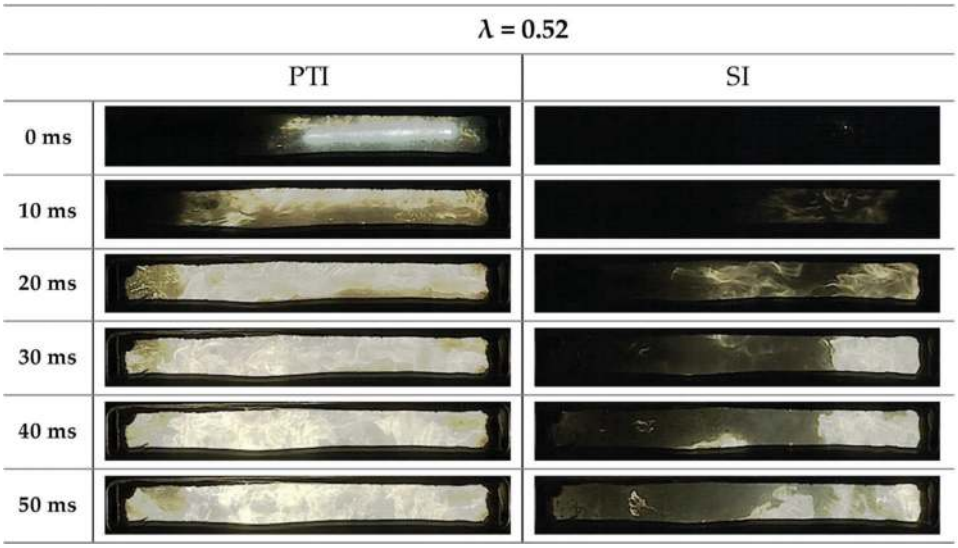

Figure 10. Pictures of the combustion process at λ = 0.52; comparison between MWCNTs/nEMs PTI and SI for air/gasoline mixture.

4. Nanostructured materials for automotive propulsion

Preliminary results from the PTI approach shows a potential for volumetrically distributed ignition of the fuels. However, the next step is to demonstrate the same results in a real engine. Indeed, the fact that a very small amount of energy (such as that emitting from an ordinary camera flash) is able to bring about volumetric ignition in a lean air/fuel mixture could lead to substantial improvements of engine performance. There are several ways the nanostructured materials could be introduced into the engine, for example, either by powder injection into the intake port or through mixing it with the fuel. A system of fiberoptic cables and flash lamp could be used to direct the flash energy into the combustion chamber.

But the main issue is possible environmental impacts of nanometric carbonaceous structures in the combustion process due to possible creation of condensation nuclei for further particulate formation in the engine and from some nanostructured materials escaping the combustion process, which can end up in the atmosphere. The potential impact of combustion products on health and environment cannot be easily predicted at the present stage of the research. In fact, it is expected that the in actual application, a more precise control of ignition timing and a shorter combustion would allow more flexibility to redesign the engine in terms of geometric as well as control parameters. This could have direct implications on the raw pollutant levels. Special concern exists because of emission of particles or particulate matters. On the other hand, many direct injection engines currently present on the market are already equipped with filtering systems, like diesel particulate filter, for the particulate abatement.

5. Conclusions

The presented data here demonstrate the feasibility of a new ignition concept for initiating the combustion process of several air/fuel mixtures. The new ignition concept is called photo-thermal ignition (PTI) and consists of flashing a nanoenergetic material with a light flash. The results from the PTI approach were compared with those obtained using a traditional spark plug system, showing great potential for future applications in combustion processes, especially for implementing the HCCI combustion mode in internal combustion engines.

In this chapter, the promising results in enhancing the combustion of methane, hydrogen, LPG, and gasoline applying this novel approach to initiate combustion are shown. In particular, the abovementioned fuels have been mixed with air in a constant volume vessel and ignited with nanopowder or a conventional spark ignition system.

The new light-activated distributed ignition demonstrated superior performance, which includes a shorter combustion duration, a shorter ignition delay period, an increased pressure peak, and improved combustion efficiency. A direct observation of the combustion process has established that benefits shown here are due to the fact that photo-thermal ignition system establishes a spatially distributed ignition, which consequently leads to a faster consumption of the air/fuel mixture in the test vessel. Higher pressure peaks and shorter rapid rising period are achieved by the fact that the new ignition system leads to numerous ignition nuclei that burn near-simultaneously, hence contributing to a volumetrically distributed combustion process in the combustion chamber. This is drastically different than the flame front propagation observed with the spark ignition.

Moreover, it was demonstrated for the first time that the proposed ignition system is able to ignite air/gasoline mixtures when liquid gasoline fuel is injected into the chamber, without isolating/encapsulating the nanoenergetic material.

Furthermore, a combustion process triggered by the photo-thermal ignition was possible even at a relative air/fuel ratio of 2.7. Ignition at this relative air/fuel ratio was impossible with the conventional spark-plug ignition system used here.

High-speed camera images acquired during the combustion process indicate that photo-thermal ignition resulted in volumetrically distributed quasi-homogeneous ignition followed by a better and faster consumption of the air/fuel mixture with no discernible flame front. This behavior is in contrast to what observed with the spark ignition, namely a single ignition point followed by a flame propagation across the combustion chamber.

The use of the photo-thermal ignition system is therefore a promising technology for the combustion management in internal combustion engines because it is characterized by the following advantages compared to the other ignition systems:

- the ignition could be achieved remotely and distributed spatially at a large number of locations; and
- the volume where ignition takes place could be adjusted to achieve both localized and volumetrically distributed ignition.

These results are considered to be of scientific and practical importance because the combustion process, initiated in mixtures with extremely lean air/fuel ratios of interest in lean-burn HCCI engines, would allow substantial reductions of fuel consumption, nitrogen oxides, and soot emissions.

Author details

Antonio Paolo Carlucci[1]*, Bruce Chehroudi[2], Antonio Ficarella[1], Domenico Laforgia[1] and Luciano Strafella[1]

*Address all correspondence to: paolo.carlucci@unisalento.it

1 Department of Engineering for Innovation, University of Salento, Lecce, Italy

2 Department of Mechanical Engineering, Arkansas Tech University, Russellville, Arkansas, USA

References

[1] Yao M, Zheng Z, Liu H. Progress and recent trends in homogeneous charge compression ignition (HCCI) engines. Progress in Energy and Combustion Science. 2009;**35**:398-437

[2] Zhao H, editor. HCCI and CAI Engines for the Automotive Industry. Woodhead Publishing in Mechanical Engineering and CRC Press; 2007. p. 557

[3] Chehroudi B. Activation and control of autoignition in HCCI engines using volumetrically-distributed ignition of as-produced single-walled carbon nanotubes. In: SAE Technical Paper. 2012. DOI: 10.4271/2012-01-1691

[4] Johansson B. Homogeneous charge compression ignition: the future of IC engines?. International Journal of Vehicle Design. 2007;**44**:1-19

[5] Iijima S. Helical microtubules of graphitic carbon. Nature. 1991;**354**:56-58

[6] Ajayan PM, Terrones M, de la Guardia A. Nanotubes in a flash-ignition—Ignition and reconstruction. Science 2002;**296**:705

[7] Tseng S, Tai N, Hsu W, Chen L, Wang J, Chiu C. Ignition of carbon nanotubes using a photoflash. Carbon. 2007;**45**(5):958-964

[8] Bockrath B, Johnson JK, Sholl DS, Howard B, Matragna C, Shi W. Ignition nanotubes with a flash. Science. 2002;**297**(5579):192-193

[9] Braidy N, Botton GA, Adronov A. Oxidation of Fe nanoparticles embedded in single-walled carbon nanotubes by exposure to a bright flash of white light. Nano Letters. 2002;**8**:1277-1280

[10] Smits J, Wincheski B, Namkung M, Crooks R, Louie R. Response of Fe powder, purified and as-produced HiPco single-walled carbon nanotubes to flash exposure. Materials Science and Engineering: A (Structural Materials: Properties, Microstructure and Processing). 2003;**358**:384-389

[11] Berkowitz A, Oehlschlaeger M. Photo-induced ignition of quiescent ethylene/air mixtures containing suspended carbon nanotubes. Proceedings of the Combustion Institute. 2011;**33**(2):3359-3366

[12] Manaa R, Mitchell A, Garza R. Flash ignition and initiation of explosives nanotubes mixture. Journal of the American Chemical Society. 2005;**127**:13786-13787

[13] Badakhshan A, Danczyk SA, Wirth D, Pilon L. Ignition of liquid fuel spray and simulated solid rocket fuel by photo-ignition of carbon nanotubes utilizing a camera flash. In: JANNAF-Liquid Propulsion Conference 2011; December 5-9; Huntsville, Alabama. 2011

[14] Chehroudi B. Nanotechnology and applied combustion: Use of nanostructured materials for light-activated distributed ignition of fuels with propulsion applications. Recent Patents on Space Technology. 2012;**1**(2):107-122

[15] Chehroudi B, Vaghjiani GL, Ketsdever A. Method for distributed ignition of fuels by light sources. US Patent 7517215 B1. 2009

[16] Chehroudi B, Vaghjiani GL, Ketsdever A. Apparatus for distributed ignition of fuels by light sources. US Patent 7665985 B1. 2010

[17] Chehroudi B, Badashan A, Danczyk SA, Morgan C. Ignition characteristics of Single-Walled Carbon Nanotubes (SWCNTs) utilizing a camera flash for distributed ignition of liquid sprays. In: Joint Army-Navy-NASA-Air Force (JANNAF) Propulsion Meeting (JPM) and 6th Modeling and Simulation/4th Liquid Propulsion/3ed Spacecraft Propulsion Joint Sub-committee Meeting; December 8-12; Orlando, Florida. 2008

[18] Chehroudi B, Danczyk SA. A novel distributed ignition method using single-walled carbon nanotubes (SWCNTs) and a low-power flash light. In: Global Powertrain Congress, World Powertrain Conference & Exposition; September 19-21; Novi, Michigan. 2006

[19] Chehroudi B, Danczyk SA, Ketsdever A, Vaghjiani GL. A low power, novel ignition of fuels using Single-Walled Carbon Nanotubes (SWCNTs) and a camera flash. In: 53ed JANNAF Interagency Propulsion Committee Meeting, 2nd Liquid Propulsion, 1st Spacecraft Propulsion Subcommittee; December 5-8; Monterey, California. 2005

[20] Chehroudi B, Danczyk SA. An innovative ignition method using SWCNTs and a camera flash. In: Nano Science and Technology Institute (NSTI), Nanotechnology Conference and Trade Show; May 8-12; Anaheim, California. 2005. p. 226-229

[21] Carlucci AP, Stafella L. Air-methane mixture ignition with Multi-Walled Carbon NanoTubes (MWCNTs) and comparison with spark ignition. Energy Procedia. 2015; **82**:915-920

[22] Carlucci AP, Ciccarella G, Strafella L. Multi-Walled Carbon Nanotubes (MWCNTs) as ignition agents for air/methane mixtures. IEEE Transactions on Nanotechnology. 2016;**15**(5):699-704

[23] Visconti P, Primiceri P, Longo D, Strafella L, Carlucci AP, Lomascolo M, et al. Photo-ignition process of multiwall carbon nanotubes and ferrocene by continuous wave Xe lamp illumination. Beilstein Journal of Nanotechnology. 2017;**8**:134-144. DOI: 10.3762/bjnano.8.14

[24] Ficarella A, Carlucci AP, Chehroudi B, Laforgia D, Strafella L. Multi-Walled Carbon Nanotubes (MWCNTs) bonded with Ferrocene particles as ignition agents for air-fuel mixtures. Fuel. 2017;**208**:734-745. DOI: https://doi.org/10.1016/j.fuel.2017.07.052